First principles study of the solubility of Zr in Al

Emmanuel Clouet* and J. M. Sanchez
Texas Materials Institute, The University of Texas at Austin, Austin, Texas 78712

C. Sigli
Pechiney Centre de Recherches de Voreppe, B.P. 27, 38341 Voreppe cedex, France

(Dated: January 22, 2004)

The experimental solubility limit of Zr in Al is well-known. Al_3Zr has a stable structure DO_{23} and a metastable one $L1_2$. Consequently there is a metastable solubility limit for which only few experimental data are available. The purpose of this study is to obtain by *ab-initio* calculations the solubility limit of Zr in Al for the stable as well as the metastable phase diagrams. The formation energies of several ordered compounds $Al_xZr_{(1-x)}$, all based on an fcc underlying lattice, were calculated using the FP-LMTO (Full Potential Linear Muffin Tin Orbital) method. Taking into account all the relaxations allowed by the symmetry, we found the DO_{23} structure to be the stable one for Al_3Zr. This set of results was then used with the cluster expansion in order to fit a generalized Ising model through the inverse method of Connolly-Williams. Different ways to consider volume relaxations were examined. This allowed us to calculate in the Bragg-Williams approximation the configurational free energy at finite temperature. According to the previous FP-LMTO calculations the free energy due to electronic excitations can be neglected. For the vibrational free energy of ordered structures we compared results obtained from a calculation of the elastic constants used with the Debye model and results obtained from a calculation of the phonon spectrum. All these different steps lead to a calculation of the solubility limit of Zr in Al which is found to be lower than the experimental one. The solubility limit in the metastable phase diagram is calculated in the same way and can thus be compared to the stable one.

I. INTRODUCTION

The development of methods based on the density functional theory[1,2] and of the computer power has allowed to conceive calculations of phase diagram from first principles[3,4] as an alternative to laboratory experimentations. Traditionally, only substitutional effects were considered, which was good enough to reproduce the topology of most phase diagrams. So as to obtain a more quantitative agreement with experimental data, it has been shown more recently that electronic excitations[5] as well as lattice vibrations[6,7] could play an important part in the relative stability of different phases. We chose to test the ability of these first principles methods to predict the solubility limit of Zr in an aluminium solid solution this part of the Al-Zr phase diagram being interesting because of the presence of a metastable phase.

The Al-richest intermediate phase of the Al-Zr phase diagram[55] is Al_3Zr. This compound has the DO_{23} structure which is body-centered tetragonal with eight atoms per unit cell, some of these atoms being allowed by symmetry to move along the main axis of the unit cell (Fig. 1). It is stable up to 1580±10°C.

The solubility limit of Zr in Al (fcc) is really low, the maximum solubility being 0.083 at.% at the peritectic reaction, Liquid+$ZrAl_3$ $\longleftrightarrow$ (Al). The solubilities of Zr in both liquid and solid were definitively determined by Fink and Willey[8] and the assessed phase diagram is based on their data. The solid solubility was determined from resistivity data and checked by metallography. Solid solubilities were also reported by Glazov *et al.*[9], Drits *et al.*[10] (solubilities determined by means of microstructural analysis and electric resistivity measurements), and Kuznetsov *et al.*[11] (determined from resistivity, microhardness and lattice constant measurements as well as metallography). The solubilities reported in these last studies are higher than the ones of the assessed phase diagram.

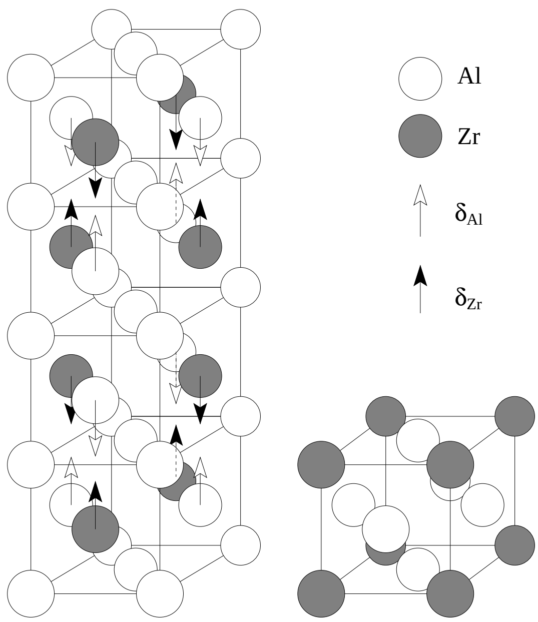

FIG. 1: Definition of the structures DO_{23} (left) and $L1_2$ (right).

Supersaturated solid solution of Zr in (Al) containing as much as 3 at.% Zr can be prepared by rapid solidification. A coherent metastable phase Al_3Zr precipitates from the supersaturated solution[12]. This phase has the structure $L1_2$ which is simple cubic with 4 atoms per unit cell (Fig. 1). This metastable phase can also form from the melt as a primary phase during rapid solidification[13,14]: Al_3Zr acts as nuclei for solidification of (Al) and Zr can thus work as a grain refiner of Al. This metastable phase is also responsible for the effectiveness of Zr to control recrystallization in Al-based alloys: it leads to a more uniform distribution of fine precipitates that pins grains and subgrains boundaries. Moreover, this phase is really stable against coarsening and redissolution, all this making it highly desirable. As few experimental data are available for this phase, it is hard to fit a thermodynamic model for it. In such a case, a first principles calculation of the phase diagram should allow us to obtain properties that are not available experimentally.

In order to assess the metastable phase diagram, we studied with the same tools and approximations the $L1_2$ and DO_{23} phases: this allows us to check first the agreement between the stable phase diagram obtained and experimental data, and then to compare it to the metastable phase diagram.

In a first part, we study the stability of ordered compounds based on an fcc underlying lattice in the Al-Zr system. The energies of different structures were calculated using an ab-initio method, the full-potential-linear-muffin-tin-orbital (FP-LMTO). The equilibrium parameters, like the volume, shape of the unit cell, or positions of atoms, were obtained. For stable structures they can be compared to experimental data.

Using this whole set of calculations we applied the cluster expansion to deduce the energy of any structure based on the same underlying lattice in the Al-Zr system, examining carefully the way to include volume relaxations.

At finite temperature, the electronic excitations, the vibrational free energy, and the configurational entropy have to be taken into account. At the end of this part, we are able to obtain a thermodynamic model written in the same way as in a Calphad approach and to calculate the corresponding solubility limits.

II. GROUND STATES OF ORDERED COMPOUNDS

Formation energies were calculated at absolute zero temperature for 26 compounds in the Al-Zr binary system, all based on an fcc lattice. Calculations were carried out using a full-potential linear-muffin-tin-orbital (FP-LMTO) method[15–17] in the version developed by Methfessel and Van Schilfgaarde[18]. The basis used contained 22 energy independent muffin-tin-orbitals (MTO) per Al and Zr site: three κ values for the orbitals s and p and two κ values for the orbitals d where the corresponding kinetic energies were $\kappa^2 = 0.01$ Ry (spd), 1.0 Ry (spd), and 2.3 Ry (sp). A second panel with a basis composed of 22 energy independent MTO with the same kinetic energies was used to make a correct treatment of the 4p semicore states of Zr. The same uniform mesh of points was used to make the integrations in the Brillouin zone for valence and semicore states. The number of divisions along reciprocal vectors was chosen big enough to ensure a convergence of the total energy of the order of 0.1 mRy/atom for each structure. The radii of the muffin-tin spheres were chosen to have a compactness of 47.6% for Al sites and 58.4% for Zr sites. Inside the muffin-tin spheres, the potential is expanded in spherical harmonics up to $l = 6$ and in the interstitial region spherical Hankel functions of kinetic energies $\kappa^2 = 1$ Ry and 3.0 Ry were fitted up to $l = 6$. The calculations were performed in the local density approximation (LDA)[1,2] and the parametrization used was the one of von Barth-Hedin[19]. Jomard *et al.*[20] showed that generalized-gradient corrections have to be included in order to obtain a correct description of the stability of the different phases of pure Zr, but as we were interested only in the Al-rich part of the phase diagram we did not include these gradient corrections.

Ground state energies at equilibrium E_0, equilibrium volumes per atom V_0, and bulk moduli B were obtained by fitting the Rose equation of state[21] to the energies calculated for different volumes around the minimum

$$E(r) = E_0 \left(1 + \frac{r - r_0}{\delta}\right) \exp\left(-\frac{r - r_0}{\delta}\right), \qquad (1)$$

where r is the Wigner-Seitz radius associated to the atomic volume V and δ is related to the bulk modulus B through the relation

$$B = \frac{-E_0}{12\pi r_0 \delta^2}. \qquad (2)$$

For the different compounds, the energies were optimized with respect to the volume and all other degrees of freedom allowed by the symmetry, like the shape of the unit cell or some atomic positions. The equilibrium volumes V_0, bulk moduli B, and formation energies E^{form} relative to the fcc phases of both pure Al and Zr are presented in table I. We note that all the formation energies are negative, and they thus characterize Al-Zr as an ordering system.

We examined more closely the stability of the phases $L1_2$, DO_{22}, and DO_{23} of Al_3Zr according to relaxations. $L1_2$ being cubic, its energy was optimized with respect to atomic volume only, whereas in the tetragonal DO_{22} phase optimization was performed additionally with respect to the c/a ratio and in the tetragonal DO_{23} phase to the c/a ratio and to the atomic displacements δ_{Al} and δ_{Zr} (δ_{Al} and δ_{Zr} are defined on Fig. 1).

Our results for Al_3Zr agree really well with the experimental ones (Table II). The equilibrium volumes obtained for the $L1_2$ and DO_{23} phases are lower than the experimental ones, but this is a known feature of LDA. This can be improved by adding gradient corrections: Colinet and Pasturel[23] using the generalized gradient approximation instead of LDA found a better agreement

TABLE I: Equilibrium volume V_0, bulk modulus B, and formation energy E^{form} for relaxed Al-Zr compounds calculated with LDA.

	Pearson symbol	Structure type	V_0 (Å^3/atom)	B (GPa)	E^{form} (mRy/atom)[a]
Al (fcc)	cF4	Cu	15.82	80.78	0.
$Al_{31}Zr$	cP32	?	15.99	82.56	−3.04
$Al_{15}Zr$	cI32	?	16.10	84.27	−6.99
Al_8Zr	tI18	V_4Zn_5	16.25	86.24	−9.77
Al_7Zr (D1)	cF32	Ca_7Ge	16.30	87.32	−14.33
Al_4Zr ($D1_a$)	tI10	$MoNi_4$	16.58	92.10	−21.12
Al_3Zr ($L1_2$)	cP4	Cu_3Au	16.12	99.59	−39.00
Al_3Zr (DO_{22})	tI8	Al_3Ti	16.60	99.65	−39.04
Al_3Zr (DO_{23})	tI16	Al_3Zr	16.35	100.05	−40.72
Al_2Zr (α)	hP3	CdI_2	18.01	87.16	−11.73
Al_2Zr (β)	tI6	$MoSi_2$	17.13	96.40	−26.19
Al_2Zr (γ)	oI6	$MoPt_2$	17.15	96.51	−26.08
AlZr ($L1_0$)	tP4	AuCu	18.15	103.33	−37.07
AlZr ($L1_1$)	hR32	CuPt	19.04	93.29	−16.50
AlZr (CH40)	tI8	NbP	18.52	100.48	−33.56
AlZr (D4)	cF32	?	18.49	92.58	−14.78
AlZr (Z2)	tP8	?	18.63	99.70	−21.03
Zr_2Al (α)	hP3	CdI_2	20.38	98.10	−10.72
Zr_2Al (β)	tI6	$MoSi_2$	19.53	104.84	−24.78
Zr_2Al (γ)	oI6	$MoPt_2$	19.44	104.05	−26.36
Zr_3Al ($L1_2$)	cP4	Cu_3Au	19.71	107.67	−27.11
Zr_3Al (DO_{22})	tI8	Al_3Ti	19.88	105.14	−23.49
Zr_3Al (DO_{23})	tI16	Al_3Zr	19.80	102.77	−25.18
Zr_4Al ($D1_a$)	tI10	$MoNi_4$	20.31	99.85	−16.30
Zr_7Al (D1)	cF32	Ca_7Ge	20.93	101.66	−7.96
Zr (fcc)	cF4	Cu	21.70	98.74	0.

[a]Reference phases are Al(fcc) and Zr(fcc).

TABLE II: Calculated volumes V_0, c'/a ratios ($c' = c/2$ for DO_{22} phase and $c' = c/4$ for DO_{23} phase), atomic displacements (normalized by c'), and ground state energies relative to the DO_{23} phase for Al_3Zr compared to previous calculations and experimental data.

	Method	V_0 (Å^3/atom)	c'/a	Atomic displacements	ΔE (mRy/atom)
$L1_2$	Present work	16.12			1.71
	FP-LMTO[22]				0.64
	VASP[23]	17.4			2.3
	Experiments[24]	17.14			1.69
DO_{22}	Present work	16.60	1.141		1.68
	FP-LMTO[22]				2.63
	VASP[23]	17.7	1.141		1.9
DO_{23}	Present work	16.35	1.087	$\delta_{Al} = -0.0021$ $\delta_{Zr} = -0.0273$	0.
	FP-LMTO[22]	16.28	1.09	$\delta_{Al} = +0.003$ $\delta_{Zr} = -0.026$	0.
	VASP[23]	17.5	1.079	$\delta_{Al} = +0.0003$ $\delta_{Zr} = -0.0101$	0.
	Experiments[22]	17.25	1.0775	$\delta_{Al} = +0.0004$ $\delta_{Zr} = -0.0272$	

with experimental data for these equilibrium volumes. After relaxing all the degrees of freedom, we see that DO_{23} is the stable phase. As been shown previously by Amador *et al.*[22] using the FP-LMTO technique too, it is not enough to consider only the relaxation of the shape of the unit cell (c/a ratio) of the phase DO_{23} to stabilize it, the atomic displacements δ_{Al} and δ_{Zr} allowed by the symmetry have to be relaxed too, otherwise $L1_2$

still has a lower energy. This was confirmed by Colinet and Pasturel[23] with calculations in the pseudopotential method, and we observed such a behaviour too. The values obtained after relaxation for these displacements are close to those measured by neutron diffraction by Amador *et al.*[22]: the sign of δ_{Al} is wrong but this relative displacement is too close from 0 to be really significant. The enthalpy of transformation from the $L1_2$ to the DO_{23} structure was measured by Desch *et al.*[24]. The experimental value ($\Delta H = -1.69$ mRy/atom) agrees really well with the value obtained from ours calculations ($\Delta H = -1.72$ mRy/atom), which was not the case of previous calculations.

For Zr_3Al, we found the phase $L1_2$ to have the lowest formation energy compared to the two other structures we investigated. This is in agreement with the experimental fact that $L1_2$ is the stable phase of Zr_3Al. For other compositions, the experimental stable structures are not based on an fcc underlying lattice, and therefore no direct comparison can be made with our calculations.

III. CLUSTER EXPANSION OF THE FORMATION ENERGY

The FP-LMTO method only allows one to calculate the energy of perfectly ordered systems which contain a few atoms per unit cell. Disordered or partially ordered systems can be modeled by super-cells, but this requires a too large computational time. Moreover, to compute the free energy of these systems, one needs to calculate the energy of every configuration. This cannot be directly done with *ab-initio* calculations and a cluster expansion has to be used. That is why in the following we will directly use the FP-LMTO calculations only for the perfectly ordered compounds Al_3Zr in the structures $L1_2$ and DO_{23}, and for the solid solution Al-Zr we will make a cluster expansion.

A. Formalism

Considering a binary crystal of N sites on a rigid lattice, its configuration can be described through an Ising model by the vector $\boldsymbol{\sigma} = \{\sigma_1, \sigma_2, \ldots, \sigma_N\}$ where the pseudo-spin configuration variable σ_p equals ± 1 if an A or B atom occupies the site p. Any structure is then defined by its density matrix ρ^s, $\rho^s(\boldsymbol{\sigma})$ being the probability of finding the structure s in the configuration $\boldsymbol{\sigma}$.

To any cluster of n lattice points $\alpha = \{i_1, i_2, \ldots, i_n\}$ is associated the following multisite correlation function

$$\zeta^s_\alpha = \mathrm{Tr}\,\rho^s \prod_{i\in\alpha} \sigma_i = \frac{1}{2^N} \sum_{\boldsymbol{\sigma}} \rho^s(\boldsymbol{\sigma}) \prod_{i\in\alpha} \sigma_i, \tag{3}$$

where the sum has to be performed over the 2^N possible configurations of the lattice.

Clusters related by a translation or a symmetry operation of the point group of the structure have the same correlation functions. Denoting D_α the number of such equivalent clusters per lattice site, or degeneracy, any configurational function f^s can be expanded in the form[25]

$$f^s = \sum_\alpha D_\alpha f_\alpha \zeta^s_\alpha, \tag{4}$$

where the sum has to be performed over all non equivalent clusters and the coefficients f_α are independent of the structure.

The usefulness of the expansion (4) rests on the fast convergence of these coefficients with the size of the clusters, *i.e.* with the number of points included in the cluster as well as the maximal distance between points inside the cluster. This allows one to truncate the sum using only a finite number of clusters. Knowing the value of the function f^s for a finite set of structures, the coefficients f_α can then be obtained using the inverse method proposed by Connolly and Williams[26], *i.e.* by a matrix inversion if the number of structures is the same as the number of clusters used in the truncated expansion. Here we used more structures than clusters and obtained the coefficients by a least square fit. We can thus check the convergence of the expansion by its ability to reproduce f^s.

Rather than doing the fit directly on the configurational function f^s, we did it on the excess function associated which is defined as

$$\Delta f^s = f^s - \frac{1+\zeta^s_1}{2} f^A - \frac{1-\zeta^s_1}{2} f^B, \tag{5}$$

where ζ^s_1 is the point correlation and f^A and f^B are the values of the function f^s for a lattice occupied by respectively only atoms A ($\zeta_1 = 1$) and atoms B ($\zeta_1 = -1$). In the case of the energy, this excess function is nothing else but the formation energy.

Using the expansion (4) we obtained

$$\Delta f^s = \sum_{\alpha, |\alpha|\geq 2} D_\alpha f_\alpha \left[\zeta^s_\alpha - \frac{1+(-1)^{|\alpha|}}{2} - \zeta^s_1 \frac{1-(-1)^{|\alpha|}}{2} \right], \tag{6}$$

where $|\alpha|$ denotes the number of points contained in the cluster α.

Applying the Connolly Williams method to the expression (6) rather than to (4) allows one to impose easily the condition that Δf^s should be equal to zero for pure A and pure B. We thus obtain the coefficients f_α only for clusters containing more than one point, the coefficients f_0 and f_1 of the empty and point clusters being then obtained by the relations

$$f_0 = \frac{f_A + f_B}{2} - \sum_{\alpha, |\alpha|\geq 2} \frac{1+(-1)^{|\alpha|}}{2} D_\alpha f_\alpha, \tag{7a}$$

$$f_1 = \frac{f_A - f_B}{2} - \sum_{\alpha, |\alpha|\geq 2} \frac{1-(-1)^{|\alpha|}}{2} D_\alpha f_\alpha. \tag{7b}$$

B. Relaxations

The volume of a structure, like any other property, depends on its configuration. But this volume enters directly in the cluster expansion as the coefficients f_α have to be calculated for a given volume. As we are generally interested in the equilibrium properties, this leads to some relaxations. In this study we will consider in two different ways these volume relaxations, the globally and totally relaxed expansions[27,28].

We first can make the cluster expansion explicitly volume dependent, writing

$$f^s(V) = \sum_\alpha D_\alpha f_\alpha(V) \zeta^s_\alpha, \tag{8}$$

where the coefficients $f_\alpha(V)$ are obtained by calculating the property f^s for different structures at the same volume V, the other degrees of freedom (shape of the unit cell and positions of atoms) being relaxed, and then by using the Connolly-Williams method. Doing such a cluster expansion for the energy, we can then deduce the equilibrium volume associated with a given configuration by minimizing with respect to the volume its energy as given by expression (8). This is known as the globally relaxed scheme and is based on the assumption that the volume occupied by every cluster is independent on its configuration. Such an assumption is questionable in cases where there is a significant difference between the atomic volumes of the constituent elements as in the Al-Zr system.

Another way to consider relaxations of the volume is to calculate the coefficients f_α from the equilibrium values $f^s(V_0^s)$ where everything included the volume is allowed to relax. The coefficients f_α are then volume independent and the values predicted by the expansion are directly the ones at equilibrium. Such a treatment is called a totally relaxed expansion. This expansion is still rigorous from a mathematical point of view since the relaxations are themselves functions of the configuration, so the relaxed structures will also be.

C. Results

1. *Total relaxations*

We first made a cluster expansion of the equilibrium volume, the bulk modulus, and the formation energy for the Al-Zr system on an fcc lattice: we are thus doing three different totally relaxed expansions. To perform the least square fit of the expansion, we used the 26 structures for which these equilibrium properties were obtained from our FP-LMTO calculations (Table I). The best agreement between our *ab-initio* calculations and their expansion has been obtained when using 17 clusters: the empty cluster {0}, the point cluster {1}, the pairs from first to seventh nearest neighbours {2,1}. . . {2,7}, seven triangles {3,1}. . . {3,7} presented in figures 2 a-g and the tetrahedron of first nearest neighbours {4,1} (Fig. 2 h). The values of the coefficients obtained for these three totally relaxed expansions are presented in table III and the errors compared to the direct calculation for the 25 structures in table IV.

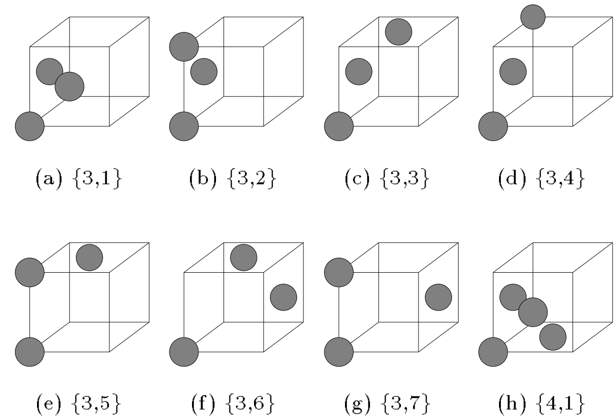

FIG. 2: Definition of the three and four points clusters on an fcc lattice used for the expansion.

TABLE III: Cluster expansion of the equilibrium volume (coefficients V_α), bulk modulus (B_α), and formation energy (J_α) in the total relaxation scheme.

Cluster	D_α	V_α (Å^3/atom)	B_α (GPa)	J_α (mRy/atom)
{0}	1	18.587	98.15	−625.05
{1}	1	−3.230	−11.12	419.87
{2,1}	6	0.149	−1.12	3.69
{2,2}	3	−0.128	1.88	−3.86
{2,3}	12	−0.013	−0.09	0.07
{2,4}	6	−0.027	−0.11	−0.15
{2,5}	12	−0.037	0.07	0.16
{2,6}	4	0.009	−0.30	0.93
{2,7}	24	0.014	−0.17	0.18
{3,1}	8	0.013	−0.14	1.74
{3,2}	12	−0.031	−0.40	−0.45
{3,3}	24	−0.001	−0.14	−0.55
{3,4}	6	0.023	0.21	−0.31
{3,5}	24	0.004	0.21	−0.33
{3,6}	24	0.010	0.14	0.22
{3,7}	24	0.005	0.06	0.54
{4,1}	2	0.030	−0.55	0.88

Looking at the cluster expansion of the formation energy, it can be seen that the maximum difference between the energy given by the expansion and the one directly obtained from the FP-LMTO calculations is 4.0 mRy/atom and that the standard deviation is 1.4 mRy/atom. We did not manage to find a better set of clusters producing a smaller error: as we still had more structures to fit than clusters, we tried to include more clusters like the pair to the eighth nearest neighbour but this did not improve the difference between our

TABLE IV: Deviations for the cluster expansion of the equilibrium volume (δV_0), the bulk modulus (δB), and the formation energy (δE^{form}) in the total relaxations scheme.

	δV_0 (Å^3/atom)	δB (GPa)	δE^{form} (mRy/atom)
Al (fcc)	0.	0.	0.
$Al_{31}Zr$	0.052	0.30	0.42
$Al_{15}Zr$	0.035	0.83	−1.02
Al_8Zr ($NbNi_8$)	0.157	−1.05	4.01
Al_7Zr (D1)	0.018	0.31	0.87
Al_4Zr ($D1_a$)	−0.012	−1.62	1.96
Al_3Zr ($L1_2$)	−0.109	−0.02	−0.21
Al_3Zr (DO_{22})	−0.029	0.63	−0.58
Al_3Zr (DO_{23})	−0.079	0.73	−2.10
Al_2Zr (α)	−0.017	0.10	−0.36
Al_2Zr (β)	−0.028	0.52	−1.11
Al_2Zr (γ)	−0.041	0.60	−1.38
AlZr ($L1_0$)	0.219	−1.18	1.96
AlZr ($L1_1$)	0.323	−0.86	0.60
AlZr (CH40)	0.077	−0.11	0.56
AlZr (D4)	−0.348	0.64	−1.20
AlZr (Z2)	0.	0.41	0.49
Zr_2Al (α)	0.011	0.03	0.16
Zr_2Al (β)	−0.007	0.46	−0.71
Zr_2Al (γ)	0.002	0.49	−0.59
Zr_3Al ($L1_2$)	−0.095	1.21	−0.32
Zr_3Al (DO_{22})	−0.038	2.01	−1.29
Zr_3Al (DO_{23})	−0.061	−2.03	−0.69
Zr_4Al ($D1_a$)	−0.012	−1.62	1.96
Zr_7Al (D1)	0.085	0.32	1.78
Zr (fcc)	0.	0.	0.
Standard deviation	0.116	0.91	1.33

FP-LMTO calculations and their expansion. Such an error does not allow one to reproduce the relative stability between different ordered compounds at a same concentration, for instance between the phases $L1_2$, DO_{22}, and DO_{23} of Al_3Zr. But as we are interested in using the cluster expansion only for the solid solution Al-Zr, this is not a problem: for perfectly ordered compounds we can directly use the results of our ab-initio calculations.

For the equilibrium volume, we can compare the accuracy of the cluster expansion with the one of the Vegard's law which assumes a linear relation between the atomic volume and the concentration. The standard deviation of the Vegard's law is 0.427 Å/atom. For none of the considered structures such an important error occurs, and we have thus obtained an important improvement by not considering only the empty and point cluster as one does in the Vegard's law.

For the bulk modulus, the accuracy of our FP-LMTO being of the order of 1 GPa, here too we can consider the convergence of the cluster expansion to be good.

2. *Global relaxations*

Using the same sets of clusters and structures, we expanded the ground state energy in 21 different volumes between 14 and 24 Å^3/atom. For each structure, these 21 expansions gave the ground state energy of the relaxed structures at the corresponding fixed volume, and we then used these results to obtain the volume, the bulk modulus, and the ground state energy at equilibrium by fitting the Rose equation of state[21].

TABLE V: Deviations for the cluster expansion of the equilibrium volume (δV_0), the bulk modulus (δB), and the formation energy (δE^{form}) obtained in the global relaxations scheme.

	δV_0 (Å^3/atom)	δB (GPa)	δE^{form} (mRy/atom)
Maximal deviation	−0.351	−2.26	5.15
Standard deviation	0.120	0.94	1.44

The maximal and standard deviations between the properties deduced from the expansion and the ones directly obtained from the FP-LMTO calculations are shown in table V. They are close to what we previously obtained in the total relaxation scheme. Actually, we did not get any important difference between the results obtained according to the way volume relaxations are considered. For each structure the deviation is quite the same in both cases, this being true for the formation energy as well as for the equilibrium volume and the bulk modulus. Such a result could not have been easily predicted as the size difference between Al and Zr is quite important: the atomic volumes given by our calculations for the fcc structures of Al and Zr are respectively 15.82 and 21.70 Å^3 (Table I). This proves that the globally and locally relaxed expansions are equivalent.

As the totally relaxed expansion only gives us one set of coefficients for the whole range of volumes, it is more convenient and we will use this expansion in the following.

IV. FINITE TEMPERATURE PROPERTIES

At finite temperature, the vibrational and electronic contributions as well as the configurational entropy have to be included in the description of the system. Considering two different time scales, a slow one for the configurational effects and a much faster for vibrations and electronic excitations[4], we define a vibrational and electronic free energy, $F^{vib}(\boldsymbol{\sigma})$ and $F^{el}(\boldsymbol{\sigma})$, both depending on the configuration. Using the variational principle, the free energy is obtained by minimizing the functional

$$F[\rho] = \langle E_0 \rangle + \langle F^{vib} \rangle + \langle F^{el} \rangle + k_B T \langle \ln \rho \rangle, \qquad (9)$$

where k_B is the Boltzmann constant and ρ the density matrix.

The cluster expansion of the formation energy at $T = 0$ K gives us an expression for the cohesive part of the functional of Eq. (9). We do not have to take into account any variation of the lattice parameter with temperature as we chose to work in the harmonic approximation: Ozoliņš and Asta[7] showed on the solubility limit of Sc in Al that there was only a small improvement when going from the harmonic to the quasiharmonic approximation. Similar expressions have to be found for the electronic and vibrational parts of the expression (9). The minimization of $F[\rho]$ with respect to ρ will then be done in the Bragg-Williams approximation.

A. Electronic free energy

At a temperature of 0 K, all electronic states of energy below the Fermi level ϵ_f are occupied, whereas the ones above are empty. At finite temperature, the electrons close to the Fermi levels can be promoted to states of higher energies according to the Fermi-Dirac distribution $f(\epsilon, T)$. The electronic excitations induce a change of the charge density and thus of the effective potential of the one electron Hamiltonian. This leads the electronic density of states (DOS) $n(\epsilon)$ to be temperature dependent. But the changes induced on the total energy and on the entropy by this temperature dependence of the electronic DOS are small[5]. We thus assumed the electronic DOS to be temperature independent and equal to the one obtained at $T = 0$. The energy change $\Delta E^{el}(T)$ and the entropy $S^{el}(T)$ due to electronic excitations are then

$$\Delta E^{el} = \int_{-\infty}^{\infty} \epsilon n(\epsilon) \left[f(\epsilon, T) - f(\epsilon, 0) \right] \mathrm{d}\epsilon, \quad (10a)$$

$$\begin{aligned} S^{el} &= -k_B \int_{-\infty}^{\infty} n(\epsilon) \left\{ f(\epsilon, T) \ln[f(\epsilon, T)] \right. \\ &\quad \left. + [1 - f(\epsilon, T)] \ln[1 - f(\epsilon, T)] \right\} \mathrm{d}\epsilon. \quad (10b) \end{aligned}$$

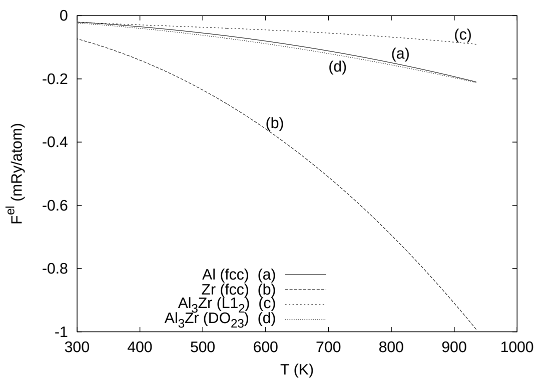

FIG. 3: Electronic free energy, $F^{el} = \Delta E^{el} - TS^{el}$.

We calculated the electronic contribution to the free energy, $F^{el} = \Delta E^{el} - TS^{el}$, for the structures Al (fcc), Zr (fcc), Al_3Zr ($L1_2$), and Al_3Zr (DO_{23}) (Fig. 3). In the range of temperature of interest, *i.e.* below 1000 K, this electronic contribution is smaller than 1 mRy/atom, and so is the excess free energy associated. This is the same range of order as the accuracy of the cluster expansion of the formation energy. We thus chose to neglect this contribution to the free energy.

B. Vibrational free energy

We studied the vibrational effects in the harmonic approximation, comparing the ability of the Debye model with a phonon calculation to predict the thermodynamic properties.

1. *Phonon calculation*

A calculation of the phonon DOS $n(\omega)$ allows one to compute the vibrational free energy. For temperatures higher than 300 K, it is enough to consider only its high temperature expression

$$\begin{aligned} F^{vib} &= k_B T \left[-3 \ln(k_B T) + \int_0^{\infty} \ln(\hbar\omega) n(\omega) \mathrm{d}\omega \right] \\ &\quad + O\left(\frac{1}{T}\right). \quad (11) \end{aligned}$$

Phonon DOS were calculated for Al (fcc), Zr (fcc), Al_3Zr ($L1_2$), and Al_3Zr (DO_{23}) in the linear response theory framework[29]. We used energy independent MTO as a basis for representing the first order correction to the one electron wave functions in the implementation developed by Savrasov[30,31]. These calculations were performed in the LDA using the parametrization of Moruzzi-Janak-Williams[32]. The radii of the muffin-tin spheres were taken equal to the ones of the band structure calculation. For valence states, the basis used was the same whereas the 4s and 4p states of Zr were treated in two different panels with the respective kinetic energies κ^2 2.7 and 1.1 mRy. For fcc structures, phonon frequencies were calculated on a grid of $8 \times 8 \times 8$ wave vectors $\vec{q}$ leading to 29 points in the irreducible Brillouin zone (IBZ), for $L1_2$ a grid of $5 \times 5 \times 5$ leading to 10 points in the IBZ was used, and for DO_{23} a grid of $4 \times 4 \times 4$ wave vectors leading to 13 points.

The calculated phonons dispersion for Al fcc is compared in figure 4 to the measurements of Stedmam *et al.*[33,34] for three different high-symmetry directions. We see that our calculation overestimates phonon frequency. Other phonon calculations for Al fcc[35–37] using the linear response theory too obtained a better agreement with experimental data. They all used a plane waves basis in the pseudopotential framework, but the use of an energy independent MTO as a basis does not seem to be the reason of the discrepancy with experimental data in our case, as Savrasov showed for Nb[30] as well as for NbC and

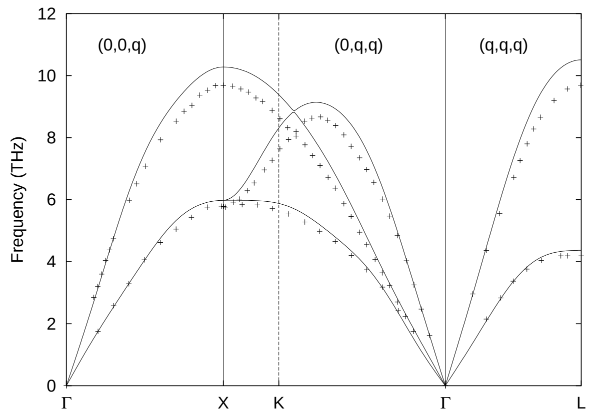

FIG. 4: Calculated phonons dispersion for Al fcc in solid line compared to experimental data (Ref.[33,34]) denoted by crosses.

Si[31] that this basis was well-suited to obtain phonon dispersion.

The phonon DOS obtained from these calculations for Al (fcc), Zr (fcc), Al_3Zr ($L1_2$), and Al_3Zr (DO_{23}) are presented in Fig. 5. For Al (fcc), we compared our calculated phonon DOS with experimental ones. Experimental DOS[34,38,39] were obtained by means of a Born-von Karman model. Force constants were fitted up to the eighth nearest neighbours in order to reproduce the phonon measurements in high-symmetry directions of Stedmam *et al.*[33,34], the Born-von Karman model being used then to compute the frequency distribution. We can see on the phonon DOS too that our calculated frequencies are slightly too high. Nevertheless, the shape of the frequency distribution is correct.

2. Debye model

The Debye model assumes a linear dispersion between the phonon frequency and its wave vector. This leads to the following high temperature expression of the vibrational free energy

$$F^{vib} = k_B T \left[-1 + 3 \ln \left(\frac{\theta_D}{T} \right) \right] + O\left(\frac{1}{T}\right), \qquad (12)$$

where the Debye temperature θ_D is obtained from the elastic constants of the structures[40].

The elastic constants were obtained by means of FP-LMTO calculations using the same set of parameters as for the formation energy calculations. The unit cell of the crystal was deformed around its equilibrium position in order to obtain the second derivative of the energy at its minimum which can be then related to the elastic tensor[41,42]. During this deformation, no relaxation was allowed. For the DO_{23} structure, the c/a ratio and the position δ_{Al} and δ_{Zr} of the atoms were frozen at their equilibrium value. For some of the deformations, we checked that these relaxations did not change much the values of elastic constants. Moreover, as we are lowering the symmetry of the structure by deforming it, some new degrees of freedom can appear, but we did not consider either these ones.

The elastic constants calculated with the FP-LMTO are compared to the experimental ones in table VI. The discrepancy between the calculated and experimental constants is in the order of 10%. This leads to some differences between the Debye temperatures obtained from these calculated constants and the ones obtained from the experimental constants, but the relative positions of these temperatures are correctly predicted.

In table VII, we show Debye temperatures obtained from a calculation of the elastic tensor for cubic structures fcc, D1, and $L1_2$ of the Al-Zr system. The structure D4 of AlZr is cubic too, but this phase was found to be mechanically unstable through a Bain deformation path and cannot be used to calculate a Debye temperature.

3. Comparison for ordered compounds

As we calculated the phonon spectrum for Al_3Zr for the stable structure DO_{23} and the metastable one $L1_2$, we were able to compare the excess vibrational free energy ΔF^{vib} obtained from the phonon DOS and the Debye model, the reference phases being Al (fcc) and Zr (fcc) (high temperature expressions are given in table VIII). We thus see that the Debye model makes an important error in predicting this excess free energy as it overestimates it by a factor ~ 2. This error comes from the inability of the Debye model to reproduce the phonon DOS as shown by figure 5. Moreover the phonon calculation shows that the two considered structures of Al_3Zr should have the same vibrational free energy which is not correctly predicted by the Debye model. This error of the Debye model would lead to a stabilization of the phase $L1_2$ at high temperatures ($T \gtrsim 905$ K) which is not true experimentally. In order to correctly describe the relative stability of these two ordered phases of Al_3Zr we cannot use the Debye model, but we need the phonon calculation.

4. Cluster expansion for the disordered phase

For the vibrational free energy of the disordered phase, we made a cluster expansion of the vibrational free energies of several ordered structures. As the Debye model only requires the calculation of the elastic tensor, which is much more faster than a calculation of the whole phonon spectrum, we used it to calculate the vibrational free energy of these ordered compounds (Debye temperatures in Table VII). By doing so we saw previously that we overestimates ΔF^{vib}, but a calculation of the phonon spectrum is not conceivable for a number of structures large enough to fit the cluster expansion. We have then to accept such an error.

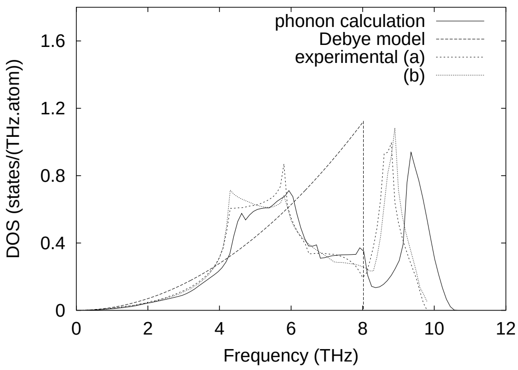

(a) Al (fcc): (a) from ref.[34,38] and (b) from ref.[34,39]

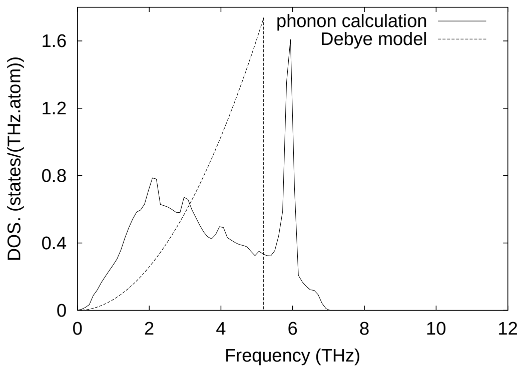

(b) Zr (fcc)

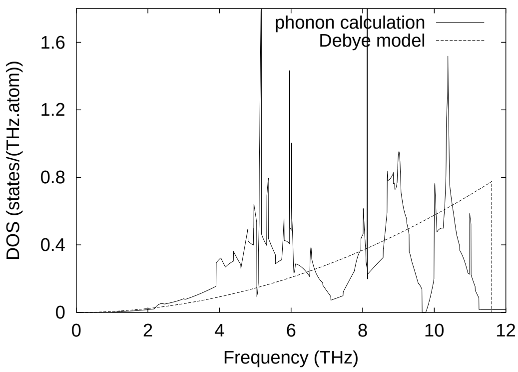

(c) Al_3Zr ($L1_2$)

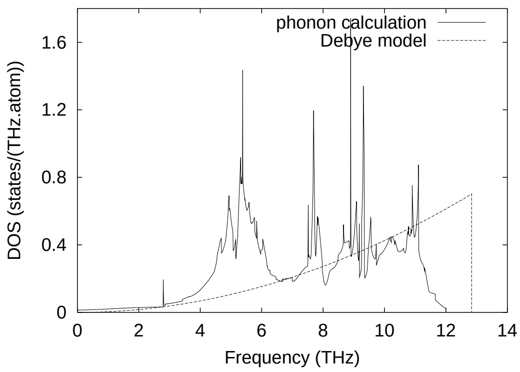

(d) Al_3Zr (DO_{23})

FIG. 5: Phonon density of state.

TABLE VI: Elastic constant C_{ij} (in GPa) calculated with the FP-LMTO compared to experimental values for Al (fcc), Al_3Zr (DO23), and Zr (hcp), and Debye temperature θ_D associated. Debye temperatures obtained by calorimetric measurements of the specific heat, when available, are given in brackets.

		C_{11}	C_{33}	C_{12}	C_{13}	C_{44}	C_{66}	θ_D (K)	
Al (fcc)	FP-LMTO	101.5	···	70.4	···	31.7	···	385	
	exp.[45,46]	114.3	···	61.9	···	31.6	···	431	(428)[43]
Al_3Zr (DO23)	FP-LMTO	215.3	228.2	54.1	33.3	103.2	123.5	616	
	exp.[47 a]	208.8	208.3	70.5	49.1	87.2	102.2	575	
Zr (hcp)	FP-LMTO	153.1	171.2	63.4	76.5	22.4	44.9	262	
	exp.[45,48]	155.4	172.5	67.2	64.6	36.3	44.1	299	(310)[44]

[a]measured at room temperature

Looking at the high temperature expression of the vibrational free energy given by the Debye model (Eq. 12), we can make the following cluster expansion

$$3 \ln \theta_D - 1 = \sum_\alpha D_\alpha J_\alpha \zeta_\alpha, \tag{13}$$

which allows us to write the vibrational free energy as

$$F^{vib} = k_B T \left[\sum_\alpha D_\alpha J_\alpha \zeta_\alpha - 3 \ln T \right]. \tag{14}$$

By doing so, the temperature dependence of the free energy is really simple and we do not have to make a cluster

TABLE VII: Elastic constants C_{ij} (in GPa) for Al-Zr compounds of cubic symmetry and Debye temperature θ_D associated.

	C_{11}	C_{12}	C_{44}	θ_D (K)
Al (fcc)	101.5	70.4	31.7	385
Al_7Zr (D1)	136.5	62.7	45.8	449
Al_3Zr ($L1_2$)	187.3	55.7	95.1	557
Zr_3Al ($L1_2$)	163.8	79.3	86.5	388
Zr_7Al (D1)	136.3	84.4	56.6	300
Zr (fcc)	121.4	87.1	45.7	249

TABLE VIII: Comparison of the high temperature expressions of the vibrational free energy obtained with the phonon calculation and the Debye model.

Al_3Zr ($L1_2$)	Phonons	ΔF^{vib}	$=$	$0.85k_BT + O\left(\frac{1}{T}\right)$
	Debye		$=$	$1.44k_BT + O\left(\frac{1}{T}\right)$
Al_3Zr (DO_{23})	Phonons	ΔF^{vib}	$=$	$0.85k_BT + O\left(\frac{1}{T}\right)$
	Debye		$=$	$1.74k_BT + O\left(\frac{1}{T}\right)$

expansion of the free energy at every temperature.

We only used four clusters in the truncated expansion: the empty cluster {0}, the point cluster {1}, the pair {2,1} of first nearest neighbours, and the triangle {3,1} of first nearest neighbours. The eight structures of table VII were used to fit the coefficients of the expansion. The results of this expansion are presented in table IX(a) and the deviations in table IX(b). Although only few clusters were used in this expansion, the convergence is really good.

TABLE IX: Cluster expansion of the function $f^s = 3\ln\theta_D - 1$ for the vibrational free energy.

Cluster	D_α	J_α
{0}	1	17.385
{1}	1	0.874
{2,1}	6	−0.197
{3,1}	8	−0.027

(a) Coefficients of the expansion.

	f^s	δf^s
Al (fcc)	16.86	0.
Al_7Zr (D1)	17.32	−0.08
Al_3Zr ($L1_2$)	17.97	0.04
Zr_3Al ($L1_2$)	16.88	0.04
Zr_7Al (D1)	16.11	−0.08
Zr (fcc)	15.55	0.

(b) Deviation δf^s of the expansion.

C. Bragg-Williams approximation

We thus obtained an expression for the different parts of the free energy functional $F[\rho]$ of expression (9): the cohesive part is given by the cluster expansion of the FP-LMTO calculations (coefficients in table III), the vibrational energy by the expression (14) with the coefficients of table IX(a), and the electronic contribution can be neglected. The functional $F[\rho]$ is minimized in the Bragg-Williams approximation. This assumes that there is no short range order and that the correlation functions can be factorized over the mean values of the pseudo spin variable $\langle\sigma_n\rangle$ for the lattice sites contained in the cluster,

$$\zeta_\alpha = \langle\prod_{i\in\alpha}\sigma_i\rangle = \prod_{i\in\alpha}\langle\sigma_i\rangle. \tag{15}$$

The Bragg-Williams approximation thus assumes that the lattice sites interact only through their mean occupancy and neglects all correlations between different sites. This can be improved by using the Cluster Variation Method (CVM)[49], but in the case of a low solubility, no really important improvement is expected when going from the Bragg-Williams approximation to the CVM. Moreover, the computational time necessary to obtain the free energy by means of the CVM increases a lot with the size of the maximal cluster. As Zr has a really low solubility in Al (fcc) and as the long range interactions of the cluster expansion of the formation energy requires a too large cluster, we chose to work with the Bragg-Williams approximation.

Within the Bragg-Williams approximation, the configurational entropy has the following expression for a binary compound

$$\begin{aligned} S[\rho] &= -k_B\sum_n(1+\langle\sigma_n\rangle)\ln(1+\langle\sigma_n\rangle) \\ &\quad +(1-\langle\sigma_n\rangle)\ln(1-\langle\sigma_n\rangle). \end{aligned} \tag{16}$$

1. *Disordered phase*

For a disordered state, all lattice sites are equivalent by symmetry. They have thus the same point correlation $\zeta_1 = 2x - 1$, where x is the Zr atomic concentration. Consequently any correlation function can be written in terms of the point correlation:

$$\zeta_\alpha = \zeta_1^{|\alpha|}. \tag{17}$$

The cluster expansion of the function f^s, using the expression (6) of the excess function Δf^s, can then be expressed as a function of the point correlation, or equally as a function of the concentration. This leads to an expression similar to the way the internal energy of a solid solution is written in a Redlich-Kister model which is of common use in the Calphad method[50]

$$f^s = xf^A + (1-x)f^B + x(1-x)\sum_{n\geq 0}L_n(2x-1)^n, \tag{18}$$

where the coefficients L_n are obtained from the coefficients J_α by the relations

$$L_n = -4\sum_{i\geq 1}\sum_{\substack{\alpha \\ |\alpha|=n+2i}} D_\alpha f_\alpha. \tag{19}$$

Using the expression (16) for the entropy, we obtain for the free energy of the disordered fcc solid solution $Al_{(1-x)}Zr_x$

$$\begin{aligned} F(x) &= (1-x)U^{Al,fcc} + xU^{Zr,fcc} \\ &+k_BT\left[x\ln x + (1-x)\ln(1-x)\right] \\ &+x(1-x)\sum_{n\geq 0} L_n(2x-1)^n. \end{aligned} \tag{20}$$

The Redlich-Kister coefficients are obtained from the cluster expansion of the formation energy and the cluster expansion of the vibrational free energy calculated in the Debye approximation.

$$\begin{aligned} L_0 &= -89.09 + 29.9\times 10^{-3}T \text{ mRy/atom} \\ L_1 &= -14.30 + 5.47\times 10^{-3}T \text{ mRy/atom} \\ L_2 &= -7.03 \text{ mRy/atom} \end{aligned} \tag{21}$$

For a dilute solution ($x \ll 1$), the expression (20) is equivalent to the free energy of a regular solution, the excess free energy being then $x(1-x)\Omega = x(1-x)(L_0 + L_1 + L_2)$. We compare in table X the value of Ω obtained from our calculations to the ones obtained by a fit of the phase diagram through a Calphad approach[51,52].

TABLE X: Parameter Ω (in mRy/atom) of the excess free energy for an fcc regular solid solution Al-Zr deduced from *ab-initio* calculations and compared to values obtained by a fit of the experimental phase diagram.

Present work	Ω	$=$	$-110.42 + 35.37\times 10^{-3}T$
Saunders[51]		$=$	$-87.60 + 22.85\times 10^{-3}T$
Murray *et al.*[52]		$=$	$-85.08 + 31.01\times 10^{-3}T$

2. Line compounds

Al_3Zr in the DO_{23} or $L1_2$ structures can be considered as a line compound, *i.e.* perfectly ordered: both structures are composed of interpenetrating sublattices of pure Al and pure Zr. The configurational entropy of such line compounds can be neglected and these structures only exist for a concentration $x = 1/4$. We checked with a calculation using the previous cluster expansions of the formation and vibrational energies that this assumption was correct in the range of temperature of interest when looking at equilibrium with the solid solution. The free energy of these compounds is then simply given by

$$F^{Al_3Zr} = \frac{3}{4}U^{Al,fcc} + \frac{1}{4}U^{Zr,fcc} + \Delta U^{Al_3Zr}, \tag{22}$$

where ΔU^{Al_3Zr} (in mRy/atom) is obtained from our previous calculations of the formation energy (Table I) and of the excess vibrational free energy calculated from the phonon DOS (Table VIII),

$$\Delta U^{Al_3Zr,L1_2} = -39.00 + 5.38\times 10^{-3}T, \tag{23a}$$
$$\Delta U^{Al_3Zr,DO_{23}} = -40.72 + 5.38\times 10^{-3}T. \tag{23b}$$

D. Solubility limit of Zr in Al (fcc)

Using the previous expressions for the free energies of the disordered phase and the line compounds Al_3Zr, we obtained the solubility limit of Zr in Al (fcc), both in the stable phase diagram when considering the structure DO_{23} for Al_3Zr and in the metastable one when considering the structure $L1_2$. As we are in the case of a dilute solid solution, the solubility limit of Zr in Al (fcc) is an analytic function of the temperature[53],

$$x = \exp\left(\frac{4\Delta U^{Al_3Zr} - \Omega}{k_BT}\right). \tag{24}$$

The solubility we obtained is too low: at the melting temperature of the perictectic it is equal to 0.0016 at.% Zr, whereas the one deduced from experimental data is 0.08 at.% Zr[52]. When comparing the variation with respect to $1/T$ of $\ln x$ with experimental measurements, we obtain a straight line having the same slope as Fink data[8] (*cf.* Fig. 6). This shows that our calculations provide an approximation of the enthalpy difference between the solid solution and the DO_{23} ordered compound which is consistent with Finks data, and that the discrepancy on the solubility limit only arises from an error on the estimation of the entropy difference. Computing the solubility limit of Sc in Al, Asta *et al.*[54] reached the same conclusion that *ab-initio* calculations correctly predicted the enthalpy difference between the ordered compound and the solid solution when compared to experimental data. In our case, the error on the entropic terms may come from an overestimation of the vibrational free energy of the disordered phase due to the use of the Debye model for this phase. As for the structures DO_{23} and $L1_2$ of Al_3Zr, the Debye model overestimates the excess vibrational free energy by a factor ~ 2 (Table VIII), we can think that we get an error of the same range for the solid solution.

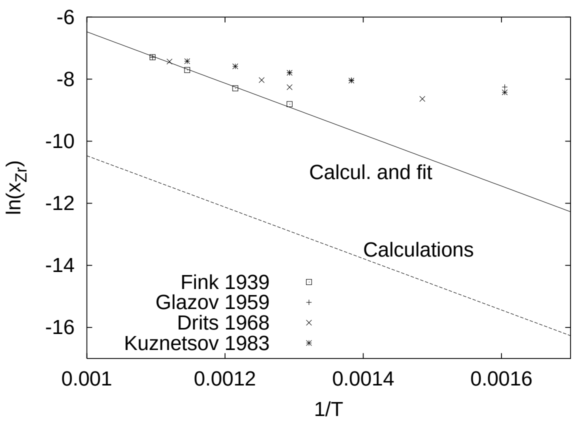

FIG. 6: Fit of the entropy of the solid solution so as to reproduce Fink experimental data.

We correct the entropic part, leaving unchanged the enthalpic part, of the parameter Ω defining the excess free energy of the solid solution so as to obtain a perfect agreement with Fink data (*cf.* Fig. 6), and we obtain

$$\Omega = -110.42 + 10.07 \times 10^{-3} T \text{ mRy/atom.} \qquad (25)$$

We thus get a stable solubility limit that is consistent with Fink measurements, and we are now able to predict the metastable limit using the expression (25) to evaluate the excess free energy of the solid solution. As the structures DO_{23} and $L1_2$ of Al_3Zr have the same vibrational free energy, the difference of solubility limit is only due to the difference of ground state energies of these two phases. At the melting temperature of the peritectic, we obtain a maximal metastable solubility limit equal to 0.275 at.% Zr.

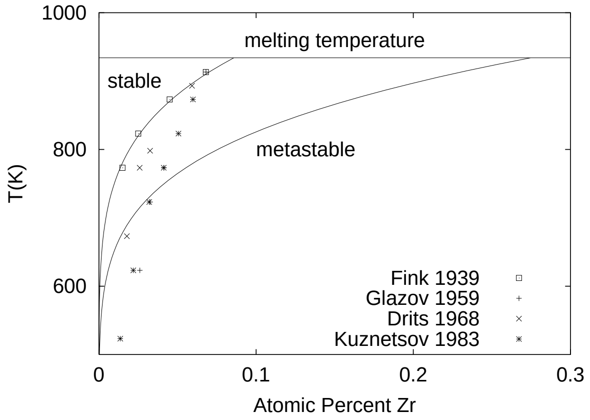

FIG. 7: Calculated stable and metastable solubility limits of Zr in Al compared to experimental data[8–11]

This is to compare to the results obtained by a Calphad method. Murray *et al.*[52] modelled the metastable phase of Al_3Zr as a line compound. They assumed that only an enthalpy term, and no entropy term, contributes to the free energy difference between the stable and metastable phases. This was done to guarantee that $L1_2$ does not become stable at high temperature. Moreover there is no experimental data that allows to estimate the entropy of the $L1_2$ phase. Our calculation of the vibrational free energy shows that such an approximation was correct. The enthalpy difference between the two compounds was assumed to arise from the coherency of the phase $L1_2$ with the matrix. They calculated from the elastic properties of Al and an estimate of the composition dependence of the lattice parameter an elastic energy of 1.52 mRy/atom. This estimation is quite close to our calculation (ΔH = 1.72 mRy/atom) as well as to the experimental measurement of Desch *et al.*[24] (ΔH = 1.69 mRy/atom). They thus obtained a solubility limit that is higher in the metastable phase diagram than in the stable one and their prevision is really close to our result: they predicted a maximal metastable solubility limit equal to 0.21 at.%.

In another Calphad study, Saunders[51] used the Gibbs energy for the disordered Al (fcc) solution, as derived from the stable equilibrium diagram, to construct the Gibbs energy of the ordered $L1_2$ phase in the Bragg-Williams approximation. He found a higher solubility limit for Zr in the metastable phase diagram than Murray *et al.* as he predicted a metastable solvus composition of 0.3 at.% Zr at the melting temperature of the peritectic.

Our study thus allows one to estimate the free energy difference between the stable and metastable phases of Al_3Zr, quantity which is not available experimentally and has to be guessed in these Calphad studies. One thus sees how it is possible to improve the thermodynamic database available to Calphad methods.

V. CONCLUSION

The equation of state for several compounds in the Al-Zr system has been computed using the full potential linear muffin tin orbital method (FP-LMTO). These *ab-initio* calculations correctly predict the stability of the phase DO_{23} for Al_3Zr if we consider the cell internal relaxations.

We made a cluster expansion of the results of *ab-initio* calculations to predict the formation energy of any compound in the Al-Zr system based on an fcc underlying lattice. We showed that despite the size difference between Al and Zr a totally or globally relaxed expansion for the volume leads to the same result: there is no difference if we use the cluster expansion to predict the formation energy at the equilibrium volume of each structure or at a fixed volume, the energy being then minimized according to the volume.

For finite temperature calculations, we showed that the electronic excitations can be neglected. The vibrational energy was studied in the harmonic model, using different levels of approximation: the Debye model was compared to results obtained from a calculation of the phonon spectrum for Al_3Zr in the structures DO_{23} and $L1_2$, and it was found that the use of the Debye model leads to an overestimation of the vibrational free energy. So we preferred to use the results from the phonon spectrum to calculate the vibrational free energy of ordered compounds. For the disordered phase, we chose to make a cluster expansion of the vibrational free energy. It was only possible with the Debye model as this requires less computational time.

We were able to calculate the solubility limit of Zr in Al (fcc) in the the Bragg-Williams approximation. The solubility limit obtained is too low compared to experimental data. We showed that this discrepancy is due to an error in the estimation of the entropy in our thermodynamic model. This may be due to an overestimation of the vibrational free energy of the disordered phase because of the use of the Debye model for this phase. Correcting the vibrational entropy of the solid solution so as to fit the experimental measurements of Fink, we were able to predict the metastable solubility limit which lies between the estimation of Murray and the one of

Saunders, both obtained by a Calphad method. We thus showed how first principles calculations can lead to an estimation of the phase diagram. This approach has the advantage of not requiring any experimental input, and consequently this is not a problem to predict stability of metastable phases.

Acknowledgments

The authors would like to thank M. Nastar for valuable discussions. Financial support from Pechiney CRV (France) is acknowledged.

---

* Electronic address: `emmanuel.clouet@cea.fr`; Current address: Service de Recherches de Métallurgie Physique, CEA/Saclay, 91191 Gif-sur-Yvette, France

[1] P. Hohenberg and W. Kohn, Phys. Rev. **136**, B864 (1964).
[2] W. Kohn and L. J. Sham, Phys. Rev. **140**, A1133 (1965).
[3] F. Ducastelle, *Order and Phase Stability in Alloys* (North-Holland Amsterdam, 1991).
[4] D. de Fontaine, Solid State Physics **47**, 33 (1994).
[5] C. Wolverton and A. Zunger, Phys. Rev. B **52**, 8813 (1995).
[6] G. D. Garbulsky and G. Ceder, Phys. Rev. B **49**, 6327 (1994).
[7] V. Ozoliņš and M. Asta, Phys. Rev. Lett. **86**, 448 (2001).
[8] W. L. Fink and L. A. Willey, Trans. AIME **133**, 69 (1939).
[9] V. M. Glazov, G. Lazarev, and G. Korolkov, Metallovedenie i Termicheskaia Obrabotka Metallov. **10**, 48 (1959).
[10] M. E. Drits, Y. S. Kadaner, and V. I. Kuz'mina, Izv. Akad. Nauk SSSR Met. **1**, 102 (1968).
[11] G. M. Kuznetsov, A. V. Barsukov, and M. I. Abas, Sov. Non-Ferrous Met. Res. **11**, 47 (1983).
[12] N. Ryum, Acta Met. **17**, 269 (1969).
[13] E. Nes, Acta Met. **20**, 499 (1972).
[14] E. Nes and H. Billdal, Acta Met. **25**, 1031 (1977).
[15] O. K. Andersen, Phys. Rev. B **12**, 3060 (1975).
[16] M. Methfessel, Phys. Rev. B **38**, 1537 (1988).
[17] M. Methfessel, C. O. Rodriguez, and O. K. Andersen, Phys. Rev. B **40**, 2009 (1989).
[18] M. Methfessel and M. van Schilfgaarde, Phys. Rev. B **48**, 4937 (1993).
[19] U. von Barth and L. Hedin, J. Phys. C **5**, 1629 (1972).
[20] G. Jomard, L. Magaud, and A. Pasturel, Philos. Mag. B **77**, 67 (1998).
[21] J. H. Rose, J. R. Smith, F. Guinea, and J. Ferrante, Phys. Rev. B **29**, 2963 (1984).
[22] C. Amador, J. J. Hoyt, B. C. Chakoumakos, and D. de Fontaine, Phys. Rev. Lett. **74**, 4955 (1995).
[23] C. Colinet and A. Pasturel, J. Alloys Comp. **319**, 154 (2001).
[24] P. B. Desch, R. B. Schwarz, and P. Nash, J. Less-Common Metals **168**, 69 (1991).
[25] J. M. Sanchez, F. Ducastelle, and D. Gratias, Physica **128A**, 334 (1984).
[26] J. W. Connolly and A. R. Williams, Phys. Rev. B **27**, 5169 (1983).
[27] A. E. Carlsson, Phys. Rev. B **35**, 4858 (1987).
[28] J. M. Sanchez, in *Structural and Phase Stability of Alloys*, edited by J. L. Morán-López, F. Mejía-Lira, and J. M. Sanchez (1992), pp. 151–165.
[29] S. Baroni, P. Giannozzi, and A. Testa, Phys. Rev. Lett. **58**, 1861 (1987).
[30] S. Y. Savrasov, Phys. Rev. Lett. **69**, 2819 (1992).
[31] S. Y. Savrasov, Phys. Rev. B **54**, 16470 (1996).
[32] V. L. Moruzzi, J. F. Janak, and A. R. Williams, *Calculated Electronic Properties of Metals* (Pergamon, New York, 1978).
[33] R. Stedman and G. Nilsson, Phys. Rev. **145**, 492 (1966).
[34] P. Dederichs, H. Schober, and D. Sellmyer, in *Landolt-Börnstein*, edited by K.-H. Hellwege and O. Madelung (Springer, Berlin, 1981), vol. III/13(a).
[35] A. A. Quong and B. M. Klein, Phys. Rev. B **46**, 10734 (1992).
[36] S. de Gironcoli, Phys. Rev. B **51**, 6773 (1995).
[37] R. Bauer, A. Schmid, P. Pavone, and D. Strauch, Phys. Rev. B **57**, 11276 (1998).
[38] E. R. Cowley, Can. J. Phys. **52**, 1714 (1974).
[39] G. Gilat and R. M. Nicklow, Phys. Rev. **143**, 487 (1966).
[40] G. A. Alers, in *Physical Acoustics*, edited by W. P. Mason (Academic, New York, 1965), vol. III-B, pp. 1–42.
[41] P. Söderlind, O. Eriksson, J. M. Wills, and A. M. Boring, Phys. Rev. B **48**, 5844 (1993).
[42] L. Fast, J. M. Wills, B. Johansson, and O. Eriksson, Phys. Rev. B **51**, 17431 (1995).
[43] N. E. Phillips, Phys. Rev. **114**, 676 (1959).
[44] N. M. Wolcott, Philos. Mag. **2**, 1246 (1957).
[45] R. Bechmann and R. F. S. Hearmon, in *Landolt-Börnstein*, edited by K.-H. Hellwege and A. M. Hellwege (Springer, Berlin, 1966), vol. III/1.
[46] G. N. Kamm and G. A. Alers, J. Appl. Phys. **35**, 327 (1964).
[47] M. Nakamura and K. Kimura, Journal of Material Science **26**, 2208 (1991).
[48] E. S. Fisher and C. J. Renken, Phys. Rev. **135**, 482 (1964).
[49] R. Kikuchi, Phys. Rev. **81**, 988 (1951).
[50] N. Saunders and A. P. Miodownik, *CALPHAD - Calculation of Phase Diagrams - A Comprehensive Guide* (Pergamon, 1998).
[51] N. Saunders, Z. Metallkd. **80**, 894 (1989).
[52] J. Murray, A. Peruzzi, and J. P. Abriata, J. Phase Equilibria **13**, 277 (1992).
[53] C. Sigli, L. Maenner, C. Sztur, and R. Shahni, in *Proceedings of ICAA-6, Aluminium Alloys* (1998), vol. 1, pp. 87–98.
[54] M. Asta, S. M. Foiles, and A. A. Quong, Phys. Rev. B **57**, 11265 (1998).
[55] The whole phase diagram has been extensively reviewed by Murray *et al.*[52]